Kinetics and Catalysis, Vol. 42, No. 5, 2001, pp. 693–702. Translated from Kinetika i Kataliz, Vol. 42, No. 5, 2001, pp. 762–772.

Catalysts Based on Fiberglass Supports: I. Physicochemical Properties of Silica Fiberglass Supports

L. G. Simonova*, V. V. Barelko, O. B. Lapina*, E. A. Paukshtis*, V. V. Terskikh*, V. I. Zaikovskii*, and B. S. Bal'zhinimaev***

** Boreskov Institute of Catalysis, Siberian Division, Russian Academy of Sciences, Novosibirsk, 630090 Russia*

*** Institute of Problems of Chemical Physics, Russian Academy of Sciences, Chernogolovka, Moscow oblast, 142432 Russia*

Received March 13, 2000

Abstract—The physicochemical properties and structure of supports prepared by leaching soda–silica fiberglass materials were studied using a set of physicochemical techniques (BET; IR spectroscopy; transmission electron microscopy; and ^{29}Si, ^{23}Na, ^{27}Al, ^{133}Cs, and ^{129}Xe (of adsorbed molecules) NMR spectroscopy). A matrix that corresponded in chemical composition to SiO_2 was formed at high degrees of leaching; however, it was considerably different from ordinary silica gels in properties. The structure and properties of this matrix are most adequately described by the model of a pseudolayer intercalation structure, which includes alternating layers of several silicon–oxygen tetrahedrons separated by narrow (<4 Å) cavities. Considerable amounts of OH groups (~5000 μmol/g) are contained in these cavities, and these OH groups are different from the surface hydroxyl groups of ordinary globular silica. Although the interlayer spaces are small, comparatively bulky cations can be intercalated into them.

INTRODUCTION

Catalytic systems based on fiberglass supports exhibit certain advantages over catalysts of traditional geometric shapes (pellets, rings, or blocks) in production technology, aerodynamic properties, and efficiency. Various woven and nonwoven fabrics can be made of thin glass fibers 3–15 μm in diameter. These materials exhibit good hydrodynamic characteristics, which are easy to control because of the regularity of woven elements and the possibility of optimizing the permeability coefficient. This makes it possible to develop catalytic reactors of a new design and to go from difficult-to-operate catalyst beds to organized (structured) beds of cartridge catalyst units. The latter are characterized by high strength, low hydraulic resistance, and improved mass and heat transfer because elementary fibers are thin [1, 2].

Attempts to use fiberglass materials of silica fibers in the production of automobile exhaust emission control catalysts were made as early as the 1970s–1980s [3–5]. Engineering solutions were proposed for the use of fiberglass as a carrier for supporting active components. Problems concerning the physicochemical properties of fiberglass materials and their effects on active components were beyond the scope of the cited patents. Research work [6], which was performed in the same years, was also devoted only to the applicability of fiberglass catalysts to gas emission control, without a detailed study of the nature of catalysts.

Note that starting glass fibers exhibit low specific surface area and porosity. Finely divided oxides are supported onto glass fibers to produce texture parameters required for carriers. These oxides either act as catalysts [3] or serve as a dispersing substrate for more valuable catalytic substances such as noble metals [7].

Another technique for increasing the surface area of silicate glass materials is the selective removal (leaching) of nonsilica components, for example, alkali and alkaline earth metals, from them [8–10]. This technique is widely used for preparing so-called porous glasses from bulk alkali borosilicate glass materials, which are characterized by chemical inhomogeneity and are prone to separation into microheterogeneous regions in sizes up to tens and hundreds of angstrom units [11]. Nonsilica microphases are dissolved under the action of mineral acids with the formation of pores of corresponding sizes. The Vycor technology for producing porous glass as plates, beads, and powders for various applications, in particular, in catalysis, is based on this principle [12]. Very small cavities, which are commensurable with the extracted alkali metal cations in size, are formed in homogeneous alkali silica glasses, which are simpler in composition, upon leaching. This fact is responsible for diffusion limitations both on leaching and in the use of the resulting products. Therefore, the leaching of large-sized alkali silica glass products found no practical use and is poorly known. However, the above diffusion limitations can be overcome using fine-fiber materials. Thus, a wide variety of different glasses can be used as starting materials for the production of supports.

In recent years, interest in catalysts on fiberglass supports was rekindled. In a series of works [13–16], it was found that fiberglass catalytic systems can be efficiently used in many gas-phase and liquid-phase cata-

0023-1584/01/4205-0693$25.00

lytic processes. The effect of the initial composition of glass fibers on the properties of catalysts was noted. In a number of cases, metals supported on glass fibers exhibited a higher activity than those with commonly used supports. This was explained by the presence of specific active centers, which are formed by the surface interaction between a metal and a glass fiber [13]. However, the physicochemical properties of leached glass fibers of different compositions and their effects on the state of supported metals were not studied in detail.

To clear up these questions, we performed a series of works, in which the following problems were considered:

(1) The physicochemical properties and structure of fiberglass supports prepared by the leaching of two most commonly used types of fiberglass materials—soda–silica and borosilicate glasses;

(2) The physicochemical properties and structure peculiarities of metals (Pt and Pd) supported on the above fiberglass carriers;

(3) The catalytic properties of these systems exemplified by the reactions of complete oxidation of hydrocarbons, SO_2 oxidation to SO_3, selective hydrogenation of ethylene–acetylene mixtures, etc.

In this first communication of this series, we consider the properties of leached soda–silica fiberglass supports.

EXPERIMENTAL

Commercial fiberglass of a soda–silica glass containing 80% SiO_2, 18.5% Na_2O, and 1.5% Al_2O_3 with a fiber diameter of 7–10 μm (sample C) served as the starting material. The fiberglass was leached with a 5.5% HNO_3 solution at 90°C for 10 or 60 min, dried at 110°C, and calcined in air at 300–900°C (samples CB). For comparison purposes, silica gel (sample A) with S_{sp} = 10 m^2/g and a particle size of 0.25–0.5 mm was used. This silica gel was prepared by the Patrick method [17] from liquid glass and an acid and autoclaved at 300°C to decrease the specific surface area down to values comparable to the S_{sp} of glass fibers.

The Si, Na, and Al contents of the samples were determined by atomic absorption spectrometry using an ICP atomic emission spectrometer.

The specific surface areas were determined by BET with the use of argon (S^{Ar}) and by the Sears method [17], that is, by the titration of samples suspended in a NaCl solution with sodium hydroxide (S^{Na}). Because of the small size of the Na^+ cation, the latter method is informative in studies of finely divided and microporous silicas [17, 18].

The morphology of samples was studied by transmission electron microscopy (TEM) on JEM-100CX and JEM-2010 (200 kV; line resolution of 1.4 Å) microscopes used for obtaining medium-magnification images and high-resolution micrographs, respectively. The test samples were prepared by two procedures: without destroying glass fibers or with the use of sample grinding and suspending in ethanol followed by ultrasonic dispersion. The samples were fixed in standard copper gauzes.

The structure of initial and leached fiberglass was studied by ^{29}Si, ^{23}Na, ^{27}Al, ^{133}Cs, and ^{129}Xe (of adsorbed molecules) NMR spectroscopy. Before xenon adsorption, the samples were aged in a vacuum at 300°C for 12 h; in the other cases, the weighed samples (~1 g) were not aged before measurements.

The MAS NMR spectra were measured on a Bruker MSL-400 pulse Fourier transform NMR spectrometer (magnetic field of 9.4 T) under the conditions specified in Table 1. The magic-angle spinning (MAS) of samples was performed using a high-speed probe (NMR Rotor Consult ApS, Denmark) with silicon nitride and zirconia rotors (5 mm o.d.) at a rate of 8000–10000 rpm.

It was impossible to apply IR spectroscopy of adsorbed molecules to studies of fiberglass materials for a number of reasons. On grinding fibers to a powder, their structures are disrupted; this fact casts doubt on the adequacy of the obtained data to the properties of the starting fibers. The use of IR microscopes makes it possible to operate with samples of sizes down to 50 μm, whereas the size of the test fibers was smaller than 10 μm. Transmission modes make it possible to examine plates up to 100 μm in thickness and of sizes 10 × 10 mm or greater, which are difficult to prepare

Table 1. Conditions of measuring nuclear magnetic resonance spectra

Nucleus	Nuclear spin	Isotope content, %	Resonance frequency, MHz	Scan frequency, kHz	Pulse duration, μs	Interpulse delay, s	Scan number	Reference	Notes
^{23}Na	3/2	100	105.81	25	2	0.1	450	0.1M NaCl	MAS
^{27}Al	5/2	100	104.23	100	2	1	300	1M $Al(NO_3)_3$	MAS
^{29}Si	1/2	4.7	79.49	30	4	20	300–2000	TMS*	MAS
^{133}Cs	7/2	100	52.48	50	2	1	3000	0.1M $CsNO_3$	MAS
^{129}Xe	1/2	26.4	110.69	50	3	10	2000	Xe (P = 0 torr)	$P(Xe)_{eq}$ = 1 atm

* TMS is tetramethoxysilane.

from fibers. Diffuse-reflectance techniques cannot be used for quantitative analysis. Thus, in this work, we developed a new semiquantitative analytical method combining transmission and diffuse-reflectance techniques. For measuring the IR spectra, fibers (20–40 mg) were placed as uniformly as possible on an aluminum mirror to form a circle about 15–20 mm in diameter, and this mirror was mounted in a diffuse-reflectance cell. In this case, the total light transmitted through the sample and diffusely reflected from a layer with known thickness was measured. Under these conditions, the law of light absorption is almost identical to the law of the transmission mode because the fraction of reflected light (not passed through the sample) is as low as several percent.

The IR spectra were measured on a modernized IFS-113v spectrometer (Bruker) in the range 1100–7000 cm^{-1} with a resolution of 4 cm^{-1} at room temperature without sample preparation. All of the spectra were analyzed by deconvoluting absorption band profiles into individual Gaussian components using the ORIGIN 5.1 software. The intensity was evaluated in terms of absorbance units referred to the sample weight per 1 cm^2 of the light-beam cross section. The concentrations of OH groups (C, μmol/g) were measured starting from the OH-stretching vibrational band intensities by the equation $C = A/(A_0\rho)$ [19], where ρ (g/cm^2) is the doubled amount of the catalyst per 1 cm^2 of the light-beam cross section because light passed twice through the sample (before and after reflection from the mirror), A (cm^{-1}) is the observed integrated absorption at the test band, and A_0 (cm/μmol) is the integrated absorption coefficient. According to Peri [20], these coefficients for different absorption bands were taken to be equal to the following values:

A_0, cm/μmol	3	5	22	25
Absorption band, cm^{-1}	3737–3740	3620–3650	3400	3300

The concentrations of OH groups were evaluated with an accuracy of ±30%.

RESULTS

Effect of Leaching Conditions on Chemical Composition and Specific Surface Area

Under the test conditions of leaching, sodium was almost completely extracted even after 10 min; ~0.05% Na and ~1.5% Al_2O_3 remained in the sample, and SiO_2 was the main constituent (~98.5%). An increase in the leaching time to 60 min affected the composition and physicochemical properties of samples only slightly.

The argon specific surface area of initial and leached fiberglass was almost the same and was very low (0.8–1.2 m^2/g). This value is close to the geometric surface area of cylindrical fibers 7–10 μm in diameter (Table 2). The surface area measured by the chemisorption of sodium was equal to 23–25 m^2/g; that is, it was higher than S^{Ar} by more than one order of magnitude. Hence, it follows that the action of an acid resulted in the formation of microcavities, which are accessible to the chemisorption of small Na^+ cations and restrictedly accessible to the physical adsorption of more bulky argon molecules (kinetic diameter of ~3.8 Å). The calcination of leached fiberglass at moderate temperatures (up to 300°C) left the surface area almost unchanged. At 550°C and above, S^{Na} dramatically decreased with a comparatively small change in S^{Ar}; this is indicative of the sintering of microcavities within fibers.

According to X-ray diffraction analysis, the samples calcined in a temperature range of 110–900°C were amorphous to X-rays.

Morphology According to Electron-Microscopic Data

The TEM images of leached fiberglass exhibited smooth cylindrical fibers ~10 μm in thickness. Internal structure peculiarities are indiscernible. Only image contrast inhomogeneities of size <10 Å can be considered, which were most pronounced (changed in size and traveled) upon long exposures of dried samples to an electron beam. The contrast inhomogeneities can be associated with the presence of microcavities, which undergo radiation-thermal sintering. This was also supported by the fact that changes in the internal structure were almost not observed after the calcination of samples at 550°C, that is, when micropores were sintered to a large degree.

Table 2. Changes in the specific surface area (S) of fiberglass depending on the conditions of leaching and subsequent thermal treatment (T)

Sample	$T_{leaching}$, °C	$\tau_{leaching}$, min	S^{Ar} (m^2/g) at T(°C)				S^{Na} (m^2/g) at T(°C)			
			110	300	550	900	110	300	550	900
SV-1	90	10	1.2	–	1.1	1.0	25	25	11	4
SV-2	90	60	1.2	1.5	1.5	1.8	23	23	13	5
S	–	–	1.0	–	–	–	–	–	–	–

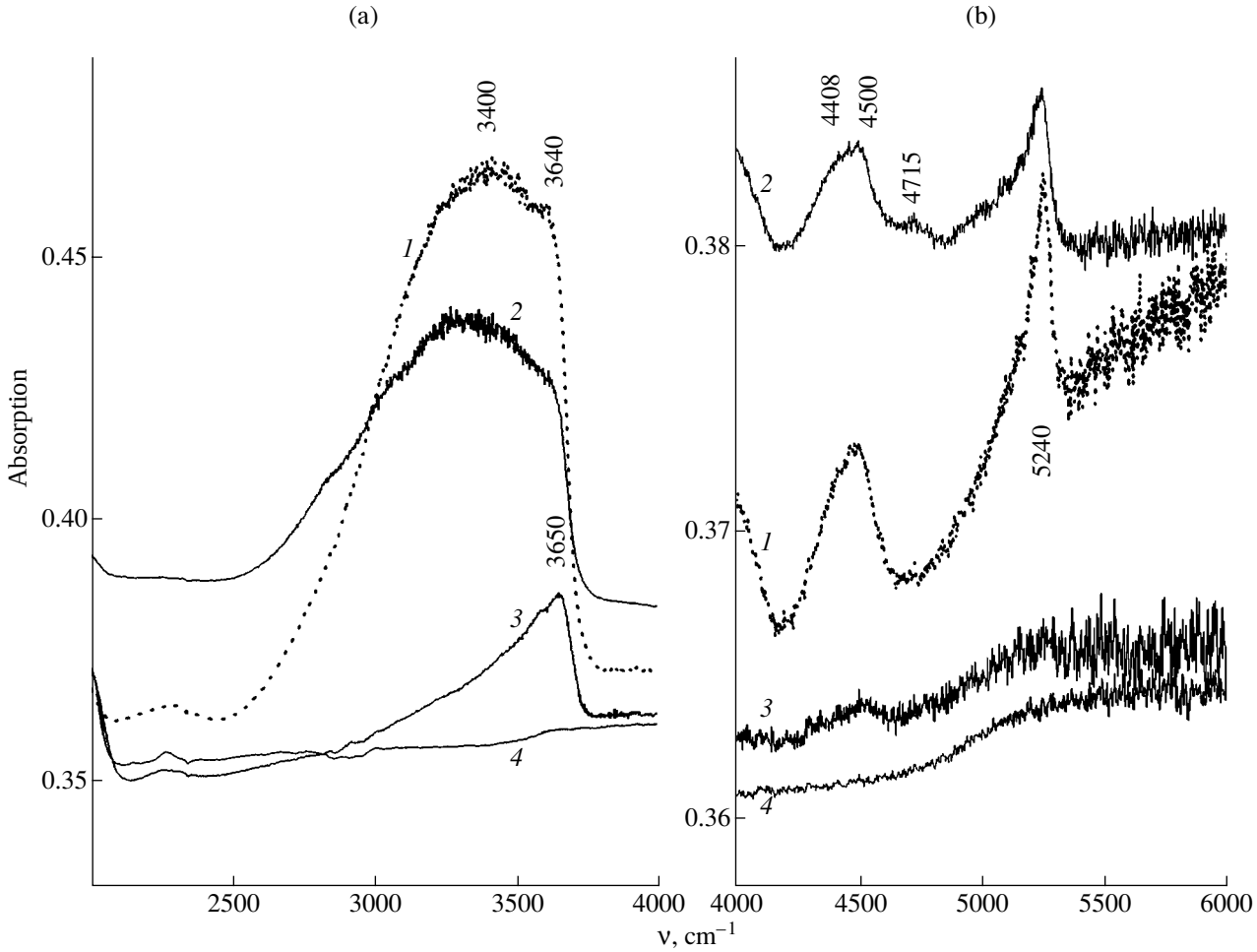

Fig. 1. IR spectra of silica fiberglass in the regions of (a) stretching and (b) combination vibrations of OH groups: (*1*) CB (110°C), (*2*) pulverized CB (110°C), (*3*) CB (550°C), and (*4*) CB (900°C). The absorption on an absorbance scale is reduced to the weight of 1 cm^2 sample (mg/cm^2). The specified vibrational frequencies were obtained by deconvoluting the spectra.

Properties of OH Groups According to IR-Spectroscopic Data

Figure 1a demonstrates the spectra of hydroxyl groups in the region of stretching vibrations for samples that were leached and calcined at different temperatures. Before leaching, the IR spectra of fiberglass exhibited only weak bands due to OH groups, whereas a fiberglass sample dried at 110°C after leaching exhibited a broad band at ~3400 cm^{-1} and a weak band at 3640 cm^{-1}. The integral intensity of these bands increased by a factor of 8–10 as compared with that of the initial sample. To elucidate the nature of OH groups and to evaluate their concentration, the observed absorption band profile was deconvoluted into individual Gaussian components. We found that a high-frequency band is relatively narrow (half-width $\Delta\nu_{1/2}$ = 80 cm^{-1}). In addition to this band, the band profile at 3400 cm^{-1} was described by a number of broad components with $\Delta\nu_{1/2}$ = 170–280 cm^{-1}. The total amount of OH groups in this sample was ~5000 μmol/g, or 1 OH group per 3 to 4 silicon atoms.

The broad band at 3400 cm^{-1} can be attributed to hydrogen-bonded OH groups. Water molecules, SiOH groups bound to water molecules with hydrogen bonds, and neighboring OH groups bound with strong hydrogen bonds in the SiOH··OHSi units usually exhibit absorption bands in this region. Because bands due to hydrogen-bonded OH groups are broad, they are difficult to separate into types. However, it is believed that the observed band at 3400 cm^{-1} is a superposition of bands due to all of the above three types of OH groups. The presence of molecular water was detected by combination bands at 5200 cm^{-1}, as described below.

The nature of a band at 3640 cm^{-1} is of interest. The low value of $\Delta\nu_{1/2}$ is indicative of the absence of hydrogen bonds. It is likely that this band is analogous to a band due to isolated OH groups on the surface of ordinary silica gels (about 3740 cm^{-1}). A decrease in its frequency by more than 100 cm^{-1} is due to the localization of these OH groups in the bulk of fiberglass or in narrow microcavities formed upon leaching. Similar

changes in silicate materials containing OH groups in the bulk of globules or in very small pores have been described in the literature [21, 22]. Unfortunately, no direct data on the structure of low-frequency (below 3700 cm^{-1}) OH groups in silicate systems are currently available. Therefore, to interpret the results, we use an analogy with bridging Si–OH–Al groups of aluminosilicates. It is reasonable that the acidity of these groups is higher than that of SiOH groups, and the positions of the corresponding absorption bands depend not only on the pore size but also on the SiOAl angle. Nevertheless, it is well known that amorphous aluminosilicates and Y-type zeolites, which are similar in acidity, exhibit the behavior described below. In an amorphous aluminosilicate, OH groups on the surface of pores with a size of 100–200 Å exhibit a band at 3740 cm^{-1}. In Y-type zeolites, absorption bands at ~3640 and ~3550 cm^{-1} correspond to hydroxyl groups localized in cavities about 12 Å in diameter and in cavities smaller than 5 Å, respectively [23]. The polarity of weakly acidic OH groups in silica gels is lower than that of OH groups in aluminosilicates; therefore, the corresponding changes in the vibrational frequencies of hydroxyl groups are exhibited at smaller pore sizes. The size of cavities in which the observed OH groups (characterized by a frequency of 3640 cm^{-1}) are localized can be estimated indirectly based on the absence of the interaction between these groups and water molecules (whose kinetic diameter is equal to 2.8 Å). The concentration of OH groups that exhibit an absorption band at 3640 cm^{-1} is ~1600 μmol/g.

After calcination at 550°C, the total amount of OH groups decreased from ~5000 to ~900 μmol/g, including ~400 and ~500 μmol/g for the band at 3650 cm^{-1} and the low-frequency wing at 3500 cm^{-1}, respectively (Fig. 1a, spectrum *3*). A further increase in the calcination temperature up to 900°C resulted in the complete dehydroxylation of the sample (Fig. 1a, spectrum *4*).

Additional information was obtained from an analysis of the spectrum in the combination region (Fig. 1b). Bands at 4400–4800 cm^{-1} are the combination bands (νOH + δ) and (νOH + νSiO), where νOH, δ, and νSiO refer to the stretching vibrations of OH groups, the bending vibrations of SiOH units, and the SiO stretching vibrations, respectively. According to published data [24, 25], bands at about 770 cm^{-1} and at about 870 cm^{-1} are assigned to SiO stretching vibrations and SiOH bending vibrations, respectively. In the specified region, vibrational modes at 4408 and 4500 cm^{-1} can be recognized for leached fiberglass.

Bands at 5100–5250 cm^{-1} are combination bands due to molecular water. They are combinations of bands due to H–O–H bending vibrations (1620–1640 cm^{-1}) and stretching vibrations, which appear at 3300–3500 cm^{-1} and overlap with bands due to SiOH groups. As can be seen in Fig. 1b (spectrum *1*), water molecules, which are characterized by a band at 5240 cm^{-1}, were present in leached sample CB(110°C). Unfortunately, the absorption coefficients for the combination bands are unknown; therefore, it is impossible to separate the combinations from molecular water and OH groups. After grinding the sample to a powder, the relative intensity of a band at 5240 cm^{-1} decreased by a factor of more than 2 (Fig. 1b, spectrum *2*), whereas bands at 4408 and 4500 cm^{-1} changed to a lesser extent, and a component appeared at 4715 cm^{-1}. For a sample calcined at 550°C, only combination bands due to SiOH groups were retained in the spectrum, whereas bands due to water disappeared (Fig. 1b, spectra *3*, *4*). All combination bands disappeared from the spectra after sample calcination at 900°C.

Table 3 summarizes the calculated vibrational frequencies δ, νSiO, and νOH in molecular water. In this case, δ and νSiO were determined by the difference between the frequencies of combination and stretching bands due to the O–SiOH unit, and νOH was found by the difference between the observed combination frequency and a bending frequency of 1620–1640 cm^{-1}. It can be seen that the bands due to SiO stretching vibrations are shifted to a high-frequency region by ~50 cm^{-1}, as compared to silica gel. Thus, it is likely that the corresponding OH groups are localized in sufficiently narrow cavities to increase the force constant of the Si–O bond because of the electrostatic repulsion of closely arranged oxygen ions.

In general, the conclusions drawn from the IR-spectroscopic data are listed below. In leached samples, OH groups are present in the bulk of fibers, and these OH groups are different from isolated OH groups on the surface of ordinary silica gels. They form weak hydrogen bonds because the frequency of stretching vibrations manifests itself at 3640 cm^{-1} (shifted by 100–110 cm^{-1}). The low value of $\Delta\nu_{1/2}$ for this band indicates that OH groups are localized in small cavities, which are uniform in geometry. Moreover, there are OH groups that

Table 3. Frequencies of the bending vibrations of SiOH groups and the stretching vibrations of water OH groups and SiO

Sample	νSiO, cm^{-1}	δ(Si–O–H), cm^{-1}	νOH(in H_2O), cm^{-1}	Notes
SiO_2(A)	770	870	–	–
SV (110°C)	820	870	3610	OH stretching vibrations in liquid water, ~3400 cm^{-1}
SV (110°C), pulverized	820	870	3600	–
SV (550°C)	820	890	–	Water molecules were absent

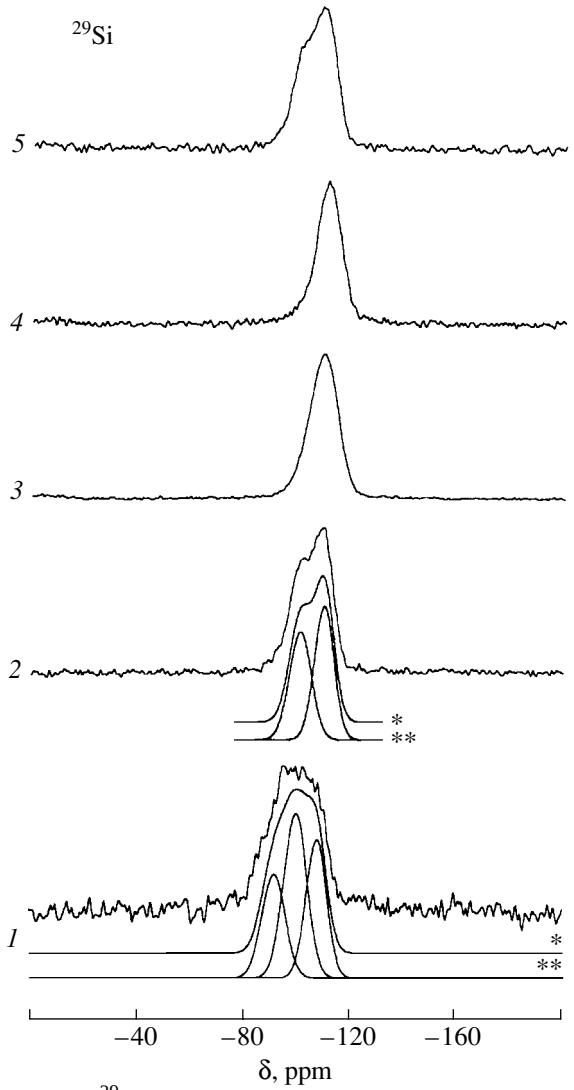

Fig. 2. ^{29}Si MAS NMR spectra of silica fiberglass: (*1*) unleached sample C, (*2*) leached sample CB (110°C), (*3*) CB (900°C), (*4*) SiO_2 (A), and (*5*) CB (110°C) + $NaNO_3$. * Simulated spectra. ** Components of the simulated spectra.

form strong hydrogen bonds (bands at 3400 cm^{-1}) and water molecules (~3600 cm^{-1}, as estimated) associated by weak hydrogen bonds. It is likely that these are individual water molecules in narrow pores. Isolated OH groups on the outer surface (3740 cm^{-1}) are not detected, probably because of a low surface area.

Table 4. Relative integral intensities of components in the ^{29}Si MAS NMR spectra of silica fiberglass

Sample	Q^2, %	Q^3, %	Q^4, %
C	30	40	30
CB (110°C)	–	45	55
CB (900°C)	–	–	100
SiO_2(A)	–	5	95

Properties of Silica Fiberglass According to NMR Data

The ^{29}Si NMR spectrum of unleached sample C exhibits a broad line with a maximum at –100 ppm (Fig. 2, spectrum *1*). According to published data [26, 27], this line can be deconvoluted into three components Q^2, Q^3, and Q^4, with chemical shifts of about –90, –100, and –110 ppm, respectively. The Q^2 line in silicate compounds is usually attributed to silicon atoms in a tetrahedral oxygen environment, which have two silicon atoms in the second coordination sphere, and the other two positions are occupied by heteroatoms like Na, H, and Al. The Q^3 state corresponds to silicon atoms having three silicon atoms and a heteroatom in the second coordination sphere. The Q^4 state refers to silicon atoms in a tetrahedral oxygen environment, of which all four atoms in the second coordination sphere are silicon atoms. Well defined positions of the lines make it possible to evaluate the fractions of the above structural states of silicon to a reasonable reliability (±15%). Table 4 summarizes the results of a computer simulation of the experimental spectrum. These data indicate that the fraction of silicon in the states $Q^2 + Q^3$ in unleached fiberglass is ~70%; that is, it is more than two times higher than the fraction of Q^4 (~30%). This is consistent with published data on the structure of Na–Si glasses with similar sodium contents [28].

The removal of sodium on leaching caused a structural change in the silicon–oxygen framework. A comparison between the ^{29}Si NMR spectra of the initial and leached fiberglass indicates that a line with a chemical shift of –90 ppm (Q^2) disappears after leaching. The spectrum becomes much narrower, and it is a superposition of two lines due to the Q^3 and Q^4 states (Fig. 2, spectrum *2*). It is believed that coordinatively unsaturated Q^2 units remained after the extraction of sodium underwent condensation to form Q^4 states. It is important that a high fraction of Q^3 states (~50%, Table 4) is typical of leached soda–silica fiberglass. In the almost complete absence of sodium (~0.05%), the presence of a Q^3 spectral component can correspond only to silanol groups Si–OH. At a Q^3 content of about 50%, the calculated OH : Si ratio is ≈0.5 or 1 OH group per 2 silicon atoms; this value is close to that obtained from the IR-spectroscopic data.

The ^{29}Si NMR spectrum of a leached sample calcined at 900°C (Fig. 2, spectrum *3*) is a symmetrical line with a chemical shift of –109 ppm, which is assigned to Q^4 structural units in the absence of Q^3 states. This can be indicative of the almost complete disappearance of silanol Si–OH groups (Q^3) on calcination because of their condensation. As can be seen in Fig. 2, the ^{29}Si NMR spectrum of sample CB(900°C) is similar to the spectrum of silica gel (A) taken for comparison. The weak downfield shoulder with a chemical shift of about –100 ppm (relative integral intensity <5%) observed in sample A can be attributed to a small amount of Q^3 groups, which occur on the surface or in the bulk. These groups contained either OH groups

(the specific surface area of silica gel is 10 m^2/g against 1 m^2/g for CB) or sodium (according to chemical analysis and NMR data, the sodium content of sample A was about 0.2%).

Xenon Adsorption

^{129}Xe NMR spectroscopy is widely used for studying microporous materials such as zeolites and clathrates [29]. A spherically symmetrical xenon atom has a kinetic diameter of 4.4 Å. A symmetry breakdown on its adsorption on a surface or on entrapment in micropores affects the parameters of ^{129}Xe NMR spectra such as line width and position [30].

We measured the ^{129}Xe NMR spectra of xenon adsorbed on leached fiberglass sample CB(110°C) at room temperature and after heating at 300°C for 5 h. Both of the spectra contained only one narrow line with a chemical sift of about 0 ppm, which corresponds to gaseous xenon present in the ampule volume between sample fibers. This fact is indicative of the absence of the physical adsorption of xenon even at an elevated temperature. At the same time, the fact that S^{Na} is higher than S^{Ar} by a factor of more than 10 is indicative that the internal volume of fibers can sorb Na^+ cations.

Ion-Exchange Properties

To study the sorption of various substances by fiberglass, we examined the ion exchange of Na^+ and Cs^+ in leached fiberglass samples calcined at 110 and 900°C and, for comparison, in silica gel A. The samples were held in $NaNO_3$ (3.5 mol/l; initial pH 6.2) and $CsNO_3$ (0.8 mol/l; initial pH 5.8) solutions at 20 and 100°C under hydrothermal conditions (Table 5). After a 4-h exposure, compounds weakly bound to the support were washed away with an ~20-fold excess of water, and the samples were dried at 110°C. The amounts and states of sorbed cations were studied by chemical analysis and NMR spectroscopy.

Starting silica gel A contained 0.2% Na. After contact with a solution of $NaNO_3$, it additionally sorbed a small amount of sodium (0.08% or 35 μmol/g) with no considerable changes in pH.

For leached sample CB(110°C) in a solution of $NaNO_3$, the pH value gradually decreased from 6.2 to 3.4 in the first 4 h and then remained almost unchanged after a day. The sodium content increased by 0.23% or ~100 μmol/g. This can be explained by the ion exchange of sodium for protons of hydroxyl groups, which are present in the bulk of fiberglass. With sample CB in contact (110°C) with a solution of $CsNO_3$, a smaller decrease in pH and a smaller amount (10 μmol/g) of sorbed cesium were observed. In ordinary silica gels, ion exchange for cesium, because of its higher basicity, proceeds in a neutral or weakly acidic region to a greater extent than that for sodium [31]. The observed decrease in the sorption of cesium in fiberglass can be explained by steric hindrances. Upon leaching sodium, commensurable cavities were formed in glass, and more bulky cesium cations can penetrate into these cavities only by increasing the size of these cavities, for example, by forcing the walls apart. It was found that the amount of sorbed cesium increased by a factor of 5 to 6 (chemical analysis and NMR data), whereas that of sodium increased by a factor of only 1.6–1.7, as the temperature increased up to 100°C. It is likely that an increase in the temperature not only enhances the diffusion of cations but also increases the flexibility of a silicon–oxygen framework [17]. Consequently, the walls of microcavities can be shifted to provide the possibility of intercalating more bulky Cs^+ cations.

A decrease in the OH-group content of samples calcined at 550–900°C diminished or terminated ion exchange for both of the cations.

Additional information on the state of alkali metals in initial, calcined, and ion-exchanged samples was obtained by ^{23}Na and ^{133}Cs NMR spectroscopy.

The ^{23}Na MAS NMR spectrum of unleached fiberglass (Fig. 3, spectrum *1*) can be represented as a super-

Table 5. Changes in the pH values of suspensions and in sodium and cesium contents after the treatment of fiberglass and silica gel with 3.5 mol/l $NaNO_3$ and 0.8 mol/l $CsNO_3$ solutions

Sample	Treatment temperature, °C	pH		Amounts of sorbed sodium or cesium	
		initial	final	wt %	μmol/g
SiO_2(A)	20	6.2	6.2	0.08	35
SV (110°C) + $NaNO_3$	″	″	3.4	0.23	100
SV (900°C) + $NaNO_3$	″	″	6.0	<0.04	17
SV (110°C) + $NaNO_3$	100	″	3.2	0.4	170
SV (110°C) + $CsNO_3$	20	5.8	4.7	0.13	10
SV (900°C) + $CsNO_3$	″	″	5.7	0.02	1.5
SV (110°C) + $CsNO_3$	100	5.8	4.1	0.66	50

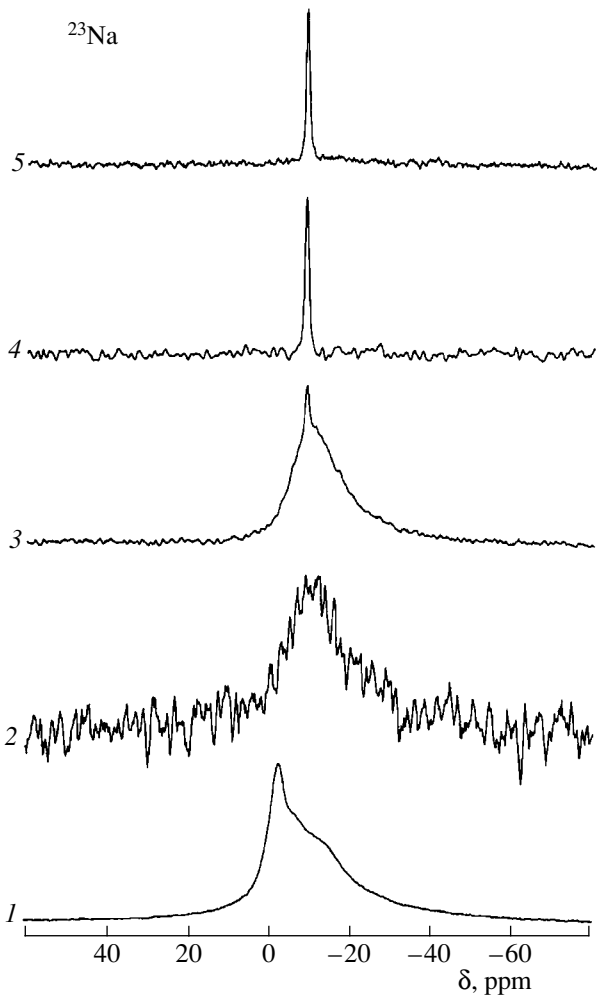

Fig. 3. ^{23}Na MAS NMR spectra of silica fiberglass: (*1*) unleached sample C, (*2*) CB (110°C), (*3*) CB (110°C) + $NaNO_3$, (*4*) CB (900°C) + $NaNO_3$, and (*5*) SiO_2 (A) + $NaNO_3$.

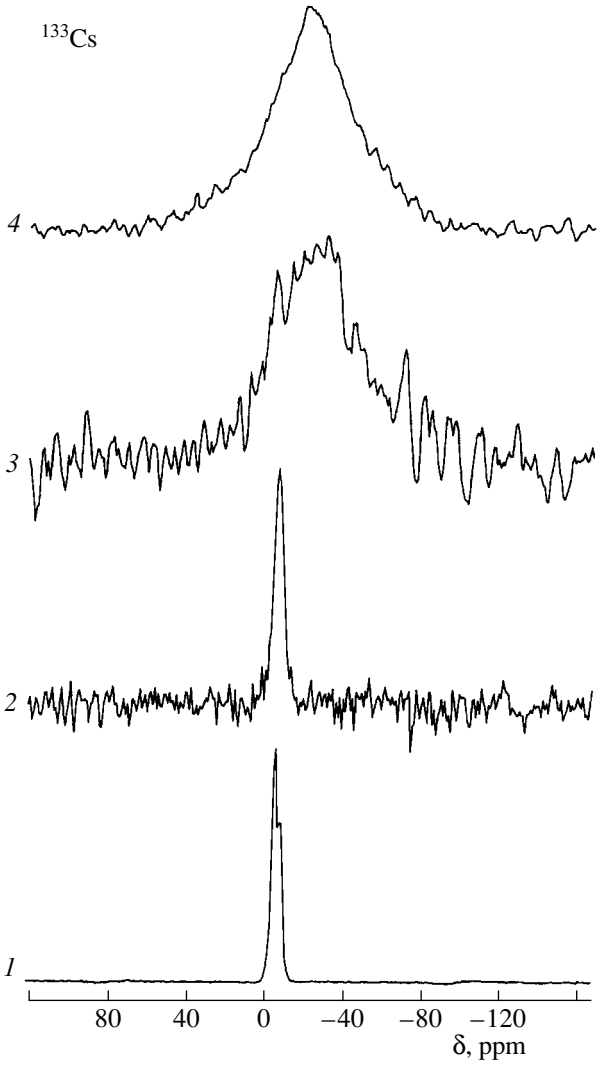

Fig. 4. ^{133}Cs MAS NMR spectra: (*1*) crystalline $CsNO_3$ salt; (*2*) SiO_2 (A) + $CsNO_3$; (*3*) CB (110°C) + $CsNO_3$, impregnation at 20°C; and (*4*) CB (110°C) + $CsNO_3$, impregnation at 100°C.

position of at least four lines with chemical shifts of –1.7, –4.4, –13.8, and –12.2 ppm. It is likely that sodium ions, binding silicon–oxygen Q^2 and Q^3 units, occupy several nonequivalent positions. In leached sample CB(110°C), the relative integral intensity of the NMR spectrum of sodium (Fig. 3, spectrum *2*) decreased to values much lower than 1% with respect to the initial sample. This fact is consistent with chemical analysis data on a high degree of leaching.

The character and intensity of spectrum *3* (Fig. 3), which was measured after sample CB (110°C) was placed in contact with sodium nitrate, indicate that the sodium content increased several times (from 0.05 to 0.23% according to chemical analysis). In this case, the state of sodium was different from that in the individual salt $NaNO_3$. At the same time, the sorption of sodium into the bulk was almost not observed in fiberglass calcined at 900°C (Fig. 3, spectrum *4*); this is consistent with chemical analysis data. An insignificant amount of crystalline sodium nitrate (a narrow line in the spectra) was detected only on the surface of fiberglass. Silica gel exhibited similar behavior. It is likely that the above increase in the sodium content of silica gel (by 0.08%) after contact with a solution of $NaNO_3$ resulted from the precipitation of an amount of sodium nitrate on the surface (Fig. 3, a narrow line in spectrum *5*) without additional sorption in the bulk.

According to ^{133}Cs NMR data, only unbound cesium nitrate was present in silica gel samples after contact with a solution of $CsNO_3$ (Fig. 4, spectra *1*, *2*). The sorption of cesium in sample CB(110°C) at room temperature was also insignificant and commensurable with the amount of cesium on silica gel (Fig. 4, spectrum *3*). However, in contrast to silica gel, cesium

enters the bulk of fiberglass, as evidenced by a broad line in the ^{133}Cs NMR spectrum (this line is similar to that in the spectra of Cs-containing glasses). The amount of cesium that entered the bulk of fiberglass increased by a factor of ~6 as the temperature increased (Fig. 4, spectrum *4*).

The ^{29}Si MAS NMR data indicate that the state of the silicon–oxygen lattice in the test samples remained almost unaffected after ion exchange for sodium or cesium.

DISCUSSION

The set of experimental data suggests that, at high degrees of leaching of soda–silica fibers, a matrix is formed that corresponds to SiO_2 in chemical composition. However, this matrix is considerably different from ordinary silica gels in structure and physicochemical properties.

First, the high concentration of silanol groups (structural units like Q^3) in leached fiberglass has engaged our attention. The Na : Si atomic ratio calculated from the ratio Q^3/Q^4 and IR-spectroscopic data is close to the ratio in unleached glass containing 18.5%Na_2O and 80%SiO_2. Note that such concentrations of surface OH groups in ordinary globular silica gels correspond to specific surface areas higher than 500 m^2/g [17]. The test samples are characterized by low surface areas measured using argon and by the absence of xenon adsorption. All of these data indicate that OH groups occur in microcavities within glass fibers. It is likely that upon leaching, all of the Na^+ cations in the glass structure were replaced with protons because of the ion exchange $Si–ONa + H^+ \longrightarrow Si–OH + Na^+$. Because protons are much smaller than sodium ions, cavities (vacancies) of a commensurable size remained at the locations of sodium [32]. The process began at the outer surface, and the leaching was easily and rapidly completed if the diameter of fibers in use was comparatively small. The dissolution front migrated to deeper cations, and the opposite diffusion flows of cations and protons formed channels that connected cavities. These channels propagated from the surface to the core, and they were separated by walls of silica, which is acid insoluble. On a macroscopic level, the channels and silicon–oxygen layers can exhibit complex irregular geometric shapes: they can be twisted and broken; their thickness can be changed because of the cross-linking of neighboring layers. However, based on the Q^3/Q^4 and OH/Si ratios, the thickness of silicon–oxygen channel walls is low and averages 4–6 silicon–oxygen tetrahedrons. Thus, the genesis is responsible for the formation of narrow but lengthy channels directed from the outer surface to the core of fibers; these channels also alternate with oriented thin silica layers. These frameworks should be structurally and behaviorally similar to intercalation layer structures. Indeed, we experimentally found that comparatively bulky cesium

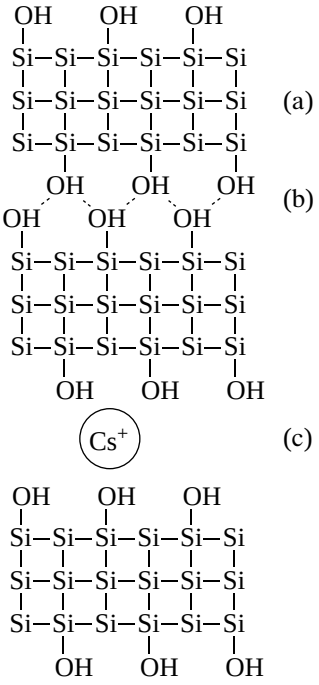

Fig. 5. Structural model of leached silica glass fibers: (a) a layer of silicon–oxygen tetrahedrons, (b) a space between the layers, and (c) a Cs^+ ion in the interlayer space upon penetrating into the bulk.

cations can penetrate into the bulk of fibers; this effect is analogous to a pillaring process in the intercalation of bulky cations in interlayer spaces with the displacement of layers [33]. As an illustration, Fig. 5 demonstrates a simplified model of the structure of leached fibers as a sectional view of a microscopic fragment. The layers of 3 to 4 silicon–oxygen tetrahedrons (for simplicity, only silicon atoms are shown) alternate with very narrow interlayer cavities in which many OH groups are present (Fig. 5b). Two neighboring silicon–oxygen layers are tightly bound with hydrogen bonds. The calcination of the material at a high temperature results in the removal of water and in the cross-linking of two layers to form a whole (a decrease in S^{Na} and in the fraction of Q^3 was observed experimentally above 550°C).

Small sodium ions easily penetrate into the interlayer space by the ion-exchange mechanism. Thus, the amounts of ion-exchanged sodium at room and elevated temperatures differed by only 60–70%. More bulky cesium cations can enter narrow interlayer spaces under conditions that activate not only the process of ion exchange but also the mobility of silicon–oxygen units.

The term *pseudolayer model* should be introduced because glass fibers are characterized by irregular structures and the absence of two-dimensional layers, which are typical of classical layer structures. What all these structures have in common is a geometric anisot-

ropy: the presence of thin silicon–oxygen elements, which are expanded deep into the fiber and hence labile. Under certain conditions, silica layers can move relative to each other, and this provides an opportunity for bulky cations to penetrate deep into glass fibers. This behavior is similar to the displacement of layers and to the pillaring effect in layered intercalation structures [33].

ACKNOWLEDGMENTS

We are grateful to A.V. Toktarev for his participation in discussions of the results and to L.A. Sergeeva for performing chemical analysis.

REFERENCES

1. Barelko, V.V., *Proc. of Int. Seminar "Block-Type Carriers and Honeycomb-Structure Catalysts,"* St. Petersburg, Russia, 1995, part I, p. 118.
2. Barelko, V.V., Khalzov, P.I., Zwiagin, V.N., and Onischenko, V.Ya., *Proc. II Conf. "Modern Trends in Chemical Kinetics and Catalysis,"* Novosibirsk, Russia, 1995, vol. II(1), p. 164.
3. US Patent 4038214.
4. JPN Patent 22145.
5. JPN Patent 137752.
6. Nicholas, D.M., Shah, Y.T., and Zlochower, I.A., *Ind. Eng. Chem. Prod. Res. Dev.*, 1976, vol. 15, no. 1, p. 29.
7. US Patent 5552360.
8. JPN Patent 51-19837.
9. US Patent 4933307.
10. RF Patent 2069584.
11. Zhdanov, S.P., *Zh. Vses. Khim. Ob-va im. D.I. Mendeleeva*, 1989, vol. 34, p. 298.
12. Yoo, J.S., Choi-Feng, Ch., and Donohue, J.A., *Appl. Catal., A*, 1994, vol. 118, no. 1, p. 87.
13. Barelko, V.V., Yuranov, I.A., Cherashev, A.V., *et al.*, *Dokl. Ross. Akad. Nauk*, 1998, vol. 361, no. 4, p. 485.
14. Kiwi-Minsker, L., Yuranov, I., Holler, V., and Renken, A., *Chem. Eng. Sci.*, 1999, vol. 54, p. 4785.
15. Dorokhov, V.G., Barelko, V.V., and Bal'zhinimaev, B.S., *Khim. Prom-st.*, 1999, no. 8, p. 44.
16. Matatov-Meytal, Yu. and Barelko, V.V., *Appl. Catal. B*, 2000, vol. 27, p. 127.
17. Iber, R.K., *The Chemistry of Silica*, New York: Wiley, 1979.
18. Fenelonov, V.B., Simonova, L.G., Gavrilov, V.Yu., and Dzis'ko, V.A., *Kinet. Katal.*, 1982, vol. 23, no. 2, p. 444.
19. Paukshtis, E.A. and Yurchenko, E.N., *Usp. Khim.*, 1983, vol. 52, no. 3, p. 426.
20. Peri, I.B., *J. Phys. Chem.*, 1966, vol. 70, p. 29.
21. Iler, R.K., *The Chemistry of Silica*, New York: Wiley, 1979.
22. Chukin, G.D., Apretova, A.I., and Sil'verstova, I.V., *Kinet. Katal.*, 1994, vol. 35, no. 3, p. 426.
23. Breck, D.W., *Zeolite Molecular Sieves*, New York: Wiley, 1976, p. 489.
24. Kustov, L.M., Borovkov, V.Yu., and Kazanskii, V.B., *Zh. Fiz. Khim.*, 1985, vol. 59, no. 9, p. 2213.
25. Tsyganenko, A.A., *Zh. Fiz. Khim.*, 1982, vol. 56, no. 9, p. 2330.
26. Mastikhin, V.M., Lapina, O.B., and Mudrakovskii, I.L., *Yadernyi magnitnyi rezonans v geterogennom katalize* (Nuclear Magnetic Resonance in Heterogeneous Catalysis), Novosibirsk: Nauka, 1992.
27. Engelharg, G. and Michel, D., *High Resolution State NMR of Silicates and Zeolites*, New York: Wiley, 1987.
28. Eckert, H., *Progr. in NMR Spectroscopy*, 1992, vol. 24, p. 159.
29. Raffery, D. and Chmelka, B.F., *NMR Basic Principles and Progress*, 1993, vol. 30, p. 111.
30. Fraissard, J. and Ito, T., *Zeolites*, 1988, vol. 8, p. 350.
31. Abendroth, R.P., *J. Colloid Interface Sci.*, 1970, vol. 34, no. 34, p. 591.
32. *Stekloobraznoe sostoyanie* (The Glassy State), Zhdanov, S.P., Ed., Leningrad: Nauka, 1983, p. 111.
33. Schollhorn., *Inclusion Compound*, Attwood, J.L., Davied, J.E., and MacNicol, D., Eds., London: Academic, 1984, p. 249.